Optical properties of (311)-oriented GaAs/AlAs superlattices

Paulo V. Santos, A. Cantarero,* M. Cardona, R. Nötzel, and K. Ploog†

Max-Planck-Institut für Festkörperforschung, Heisenbergstrasse 1, D-70569 Stuttgart, Federal Republic of Germany

The dielectric function for energies above the fundamental gap of (311)-oriented GaAs/AlAs superlattices has been investigated by ellipsometry and reflection difference spectroscopy. The superlattices have a monoclinic unit cell and are thus anisotropic in the plane of the superlattice layers. In addition, they can be grown with a periodic interface corrugation along the $[\bar{2}33]$ in-layer direction in the form of macrosteps with a height of 10.2 Å. The reduced symmetry leads to a splitting of the optical transitions, in particular of those in the energy range of the bulk GaAs E_1 and $E_1 + \Delta_1$. The observed splittings are compared to tight-binding calculations of the dielectric function.

I. INTRODUCTION

Recent advances in crystal growth have made it possible to deposit high quality GaAs/AlAs superlattices along high index growth directions, such as [011],[1] [211],[2,3] and [311],[2,3] differing from the conventional [100] growth direction. A common feature of these superlattices is the reduced symmetry as compared with the tetragonal (100)-oriented structures. As a consequence, these structures are optically anisotropic in the plane of the superlattice (SL) layers. The reduced symmetry leads to additional splittings of the optical transition[4–6] and has been probed by ellipsometry,[4] luminescence,[2,7] and reflection experiments.[8–10]

A second interesting feature of superlattices grown along directions with high indices is the appearance of a periodic interface corrugation. The interface corrugation seems to be particularly large in (311)-oriented structures.[2,3] As illustrated in Fig. 1, the corrugation in this case is composed of microsteps with a height of $\delta = 10.2$ Å repeated periodically every $d = 32$ Å in the [0$\bar{1}$1] direction. The microstep formation has been attributed to facetting of the growing GaAs and AlAs surface in order to reduce the surface free energy.[2] The

faceting depends on the growth conditions and the fabrication of (311)-oriented superlattices with flat interfaces has recently been reported.[11] The corrugation introduces an additional lateral carrier confinement in the plane of the superlattice layers. The extra confinement has been invoked to explain the energy shift of the photoluminescence spectra[3] and the lower threshold for stimulated emission[12] of (311)-oriented structures as compared to (100)-oriented superlattices.

The corrugation is also expected to yield a contribution to the in-plane optical anisotropy.[3] The optical properties and the in-plane anisotropy in the energy range of the fundamental (i.e., E_0) gap has been the subject of different theoretical and experimental investigations.[2,3,8–10,13–19] Armelles et al.[9,10] attributed the anisotropy in the piezo-reflectance of (311)-GaAs/AlAs structures only to the vertical confinement (i.e., along the growth direction) of the GaAs layers. The confinement splits the upper valence bands and leads to optical transition elements, which depend on the in-plane polarization direction. These authors concluded that the contribution of the interface corrugation to the in-plane anisotropy was negligible in their samples, in agreement with previous reflection anisotropy measurements by Belousov et al.[8] on samples with large (i.e., > 35 Å) GaAs layer thicknesses. They, however, observed an increased anisotropy when the GaAs layer thickness is reduced below 35 Å. The discrepancy was attributed to an additional anisotropy contribution from the lateral confinement as the GaAs layer thickness is reduced. More recently, an investigation of the anisotropy using photomodulation spectroscopy also identified a contribution from the lateral confinement.[19]

In this work, we investigated the optical anisotropy (311)-GaAs/AlAs superlattices using ellipsometry and reflection difference spectrocopy. In contrast to previous optical investigations,[8–10] we concentrate on the optical properties above the fundamental gap, in the energy range of the E_1 and E_2 critical points of bulk GaAs and AlAs (2–6 eV). As will be discussed in Sec. III, the dielectric function $\varepsilon = \varepsilon_1 + i\varepsilon_2$ was found to be anisotropic in the plane of the superlattice layers, with main axes
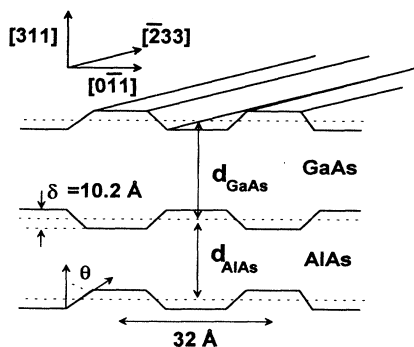
FIG. 1. Schematic representation of the interface profile in a (311)-GaAs/AlAs superlattice (Ref. 3).

along the [0$\bar{1}$1] and [$\bar{2}$33] directions. The spectral depen-
dence of $\Delta\varepsilon = \varepsilon_{[0\bar{1}1]} - \varepsilon_{[\bar{2}33]}$ in the energy range from 2 to
5 eV is characterized by sharp peaks (FWHM~ 0.15 eV)
superimposed on a structured background. The num-
ber of peaks increases and their intensities decrease with
increasing SL period. The analysis of the confinement
effects (Sec. IV A) on the states contributing to transi-
tions in the E_1 range indicate that the sharp lines are
mainly due to the vertical confinement of the GaAs lay-
ers. This conclusion is supported by tight-binding cal-
culations of the optical anisotropy performed neglecting
interface corrugation, to be presented in Sec. IV B. These
calculations reproduce the most salient structures in the
anisotropy spectrum of samples with thick GaAs lay-
ers (i.e., $d_{GaAs} > 40$ Å), indicating that they are not
directly associated with the interface corrugation. The
structured background, on the other hand, seems to be
introduced by the periodic array of macrosteps at the SL
interfaces. The spectral shape of the background is re-
produced by an effective medium approximation for the
optical anisotropy (to be presented in Sec. IV A), which
takes into account the amplitude of the surface corruga-
tion and the dielectric constant of the layers.

II. EXPERIMENTAL DETAILS

The samples studied here where grown on (311)-A-
oriented, semi-insulating GaAs substrates by molecular
beam epitaxy. Details of the growth procedure and
an x-ray characterization of the samples were presented
elsewhere.[3] Cross-section transmission electron micro-
graphs indicate the presence of the interface corrugation,
as displayed in Fig. 1.[3] The thicknesses of the individual
GaAs and of the AlAs layers, determined from the x-ray
data, ranges from 13 to 40 ML per period.

We have investigated the linear optical response of
(311)-oriented GaAs/AlAs superlattices using ellipsom-
etry and reflectance difference spectroscopy (RDS). The
ellipsometry measurements were performed with the
plane of incidence both parallel and perpendicular to the
[0$\bar{1}$1] direction (see Fig. 1). The ellipsometric angles
were converted into the pseudodielectric function, using
a two-phase model involving a sharp interface between
the sample and air. RDS was used to measure the rela-
tive difference between the complex reflection coefficient
along two perpendicular direction on the sample surface.
In the measurements linearly p-polarized light impinged
on the sample surface at quasinormal incidence (inci-
dence angle < 10°) and the polarization of the reflected
light was analyzed using an acousto-optical modulator.
Details of the experimental RDS setup are described in
details in Ref. 20. As a differential technique, RDS can
detect small anisotropies in the complex reflection coef-
ficient since the isotropic contribution is eliminated. All
experiments were performed in air and at room temper-
ature.

III. RESULTS

Figure 2(a) displays the imaginary part (left scale
of the plot) of the ellipsometric pseudo-dielectric func-
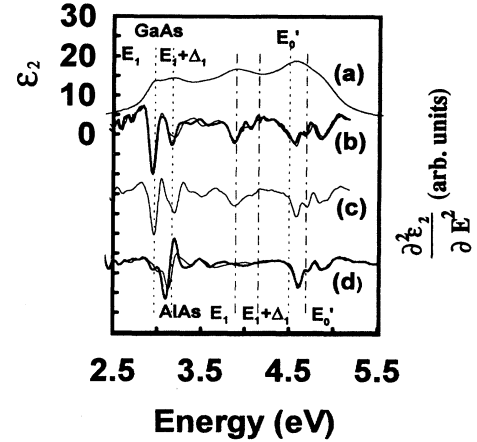
FIG. 2. (a) Imaginary part of the pseudodielectric func-
tion (left scale) for a 66 Å/61 Å (311)-GaAs/AlAs superlat-
tice. The right scale displays the imaginary part of the sec-
ond derivative with respect to the energy, Im$(\partial^2\varepsilon/\partial E)$, of the
dielectric function projection along the [0$\bar{1}$1] (thick lines) and
along the [$\bar{2}$33] optical axes (thin lines) for (311)-GaAs/AlAs
superlattices with layer thicknesses of (b) 66 Å/61 Å, (c)
43 Å/47 Å(only the [$\bar{2}$33] polarization is shown in this case),
and (d) 24 Å/22 Å.

tion (ε) of a (311)-oriented GaAs/AlAs superlattice with
GaAs and AlAs layer thicknesses of 66 and 61 Å (here-
after 66 Å/61 Å), respectively. The measurement was
performed with the [0$\bar{1}$1] surface direction of the sam-
ple aligned with the light incidence plane. According to
Ref. 21, this configuration yields in a first approximation
the dielectric tensor projections along the [0$\bar{1}$1] direction.
The main features in the spectra correspond closely to the
critical points E_1, $E_1 + \Delta_1$, E_0', and E_2 for bulk GaAs
and AlAs, indicated by the dashed and dot-dashed lines,
respectively. These features are similar to those observed
in [100]-GaAs/AlAs superlattice with the same average
composition and period length.[22]

Finer details of the optical properties become visible in
the second derivative of the *imaginary part* of the dielec-
tric constant with respect to the energy, $\partial^2\varepsilon_2/\partial E^2$. The
thick and the thin lines in Figs. 2(b)–(d) represent the
tensor projections $\partial^2\varepsilon_{2,[0\bar{1}1]}/\partial E^2$ and $\partial^2\varepsilon_{2,[\bar{2}33]}/\partial E^2$ for
samples with different layer thicknesses. For an isolated
critical point, the minima in $\partial^2\varepsilon_2/\partial E^2$ correspond closely
to the critical point energy. For superlattices with large
layer thicknesses [Fig. 2(b)] the minima in $\partial^2\varepsilon_2/\partial E^2$
agree with the energies of the bulk critical points E_1,
$(E_1 + \Delta_1)$, E_2, and E_0' of GaAs and AlAs, indicated by the
vertical dashed and dot-dashed lines, respectively. Con-
trary to the bulk, the minima are polarization dependent
with $\partial^2\varepsilon_{2,[\bar{2}33]}/\partial E^2$ shifted to higher energies in compar-
ison to $\partial^2\varepsilon_{2,[0\bar{1}1]}/\partial E^2$. With decreasing layer thickness,
the positions of the E_1-like and $(E_1 + \Delta_1)$-like minima
blueshift (see Table I) and the polarization dependence
accentuates. Note in Table I that the largest energy shifts
occurs for samples with GaAs layer thicknesses below 40
Å.

TABLE I. Transition energies for the E_1-like and $(E_1 + \Delta_1)$-like critical points in (311)-oriented GaAs/AlAs superlattices with different layer thicknesses.

Layer thicknesses (Å) (Å)	Inc. Plane	E_1-like (eV)	$(E_1 + \Delta_1)$-like (eV)
24/22	[0$\bar{1}$1]	3.1	3.33
24/22	[$\bar{2}$33]	3.14	3.39
43/47	[$\bar{2}$33]	2.97	3.19
66/61	[0$\bar{1}$1]	2.95	3.16
66/61	[$\bar{2}$33]	2.95	3.2

The optical anisotropy of the (311)-oriented superlattices can be easily detected by measuring the reflection anisotropy under quasinormal incidence. The thick lines in Fig. 3 illustrate the imaginary (upper curve) and the real (lower curve) parts of the difference in the complex reflection coefficient for polarization along the [0$\bar{1}$1] and [$\bar{2}$33], $\Delta r/r = 2(r_{[0\bar{1}1]} - r_{[\bar{2}33]})/(r_{[0\bar{1}1]} + r_{[\bar{2}33]})$, for a 42 Å/47 Å GaAs/AlAs superlattice. The [0$\bar{1}$1] and [$\bar{2}$33] axes are the principal in-plane optical axes of the (311)-oriented superlattices and the structures in the spectrum are due to the difference in the optical properties along the these two directions. This conclusion is further supported by the fact that when the sample is rotated by 45°, so as to record the difference between the complex reflectivity between two axes halfway between the main axes, a structureless spectrum is obtained, as is illustrated by the thin lines in Fig. 3 (the linear increase in the imaginary part for both spectra in Fig. 3 is an artifact of the measurements associated with nonidealities of the optical components). The main structures in $\Delta r/r$, with maximum amplitude of $\sim$ 0.5%, lay in the energy range of the E_1 and E_2 optical gaps of bulk GaAs and AlAs (i.e., between 2.9 and 5 eV). Below 2 eV, the superlattices

are partially transparent and the oscillations in the spectrum are due to interference fringes in the total superlattice film thickness. These interferences, which are much weaker when the sample is rotated by 45° (thin lines in Fig. 3), are also a direct consequence of the in-plane optical anisotropy. Superposed on the interferences are additional features associated with the fundamental (E_0) gap of the GaAs layers. The optical anisotropy in this energy range was previously investigated by Belousov et al.[8] and will not be further discussed here.

Figure 4 displays the imaginary part of the difference $\Delta\epsilon = \epsilon_{[0\bar{1}1]} - \epsilon_{[\bar{2}33]}$ for samples with different periods. $\Delta\epsilon$ was obtained by combining the ellipsometric and the reflection difference data using the expression:[23,24]

$$\frac{\Delta\epsilon}{\bar{\epsilon}} = \frac{\epsilon_{[0\bar{1}1]} - \epsilon_{[\bar{2}33]}}{\bar{\epsilon}} = \frac{(\bar{\epsilon}-1)}{\sqrt{\bar{\epsilon}}}\frac{r_{[0\bar{1}1]} - r_{[\bar{2}33]}}{\bar{r}}, \quad (1)$$

where $\bar{\epsilon} = (\epsilon_{[0\bar{1}1]} + \epsilon_{[\bar{2}33]})/2$ and $\bar{r} = (r_{[0\bar{1}1]} + r_{[\bar{2}33]})/2$. Equation (1) is strictly valid only for a uniaxial crystal. Due to the large refractive index, the incoming light propagates almost parallel to the growth axis, so that the anisotropy perpendicular to this axis can be neglected, and the superlattice can be treated as a uniaxial medium. Equation (1) allows a high-accuracy determination of the dielectric anisotropy directly from the reflection difference data.

The dielectric anisotropy is characterized by sharp peaks between 2.5 and 4.5 eV. The main feature in the

FIG. 3. Real (left scale) and imaginary part (right scale) of the reflection difference signal $\Delta r/r = 2(r_{[0\bar{1}1]} - r_{[\bar{2}33]})/(r_{[0\bar{1}1]} + r_{\bar{2}33]})$, between the two principal optical axes [0$\bar{1}$1] and [$\bar{2}$33] (thick lines), and between two axes (thin lines) located halfway between the main axes.
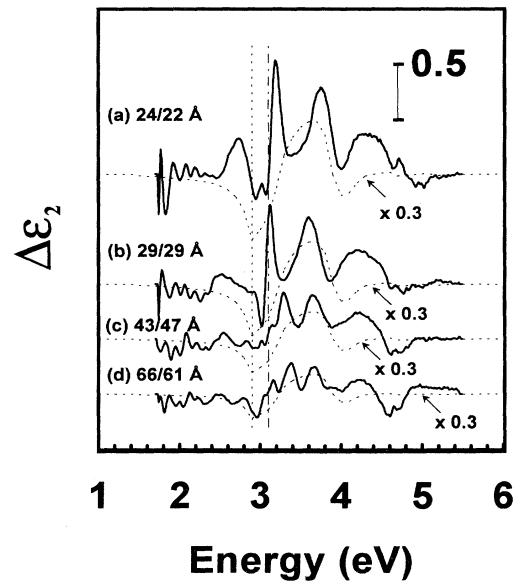
FIG. 4. Imaginary part of the difference $\Delta\epsilon$ between the dielectric constant in the [0$\bar{1}$1] and [$\bar{2}$33] in (311)-oriented GaAs/AlAs superlattices. The thickness of the superlattice layers is indicated as nn/mm, where nn (mm) is the number of GaAs (AlAs) monolayers per superlattice period. The dashed lines are the predictions of an effective medium approximation for $\Delta\epsilon$ (see text for details). The vertical dotted and dot-dashed lines indicate the energy of the bulk GaAs E_1 and $E_1 + \Delta_1$ critical points, respectively.

spectra lies close to that of the bulk GaAs E_1 and $E_1+\Delta_1$ gaps, which are indicated by the vertical lines in Fig. 4. The intensity of the sharp peaks increase with decreasing superlattice period. These results indicate that the optical anisotropy of the higher transitions is also determined by confinement effects, as has been previously demonstrated for [110]-oriented structures,[4] and also by the increasing role of lateral confinement for small layer thickness (see below).

The line shape of the anisotropy spectra near 3.1 eV changes considerably when the GaAs layer thickness is reduced below 30 Å [see structures indicated by arrows in Figs. 4(a) and (b)]. We attribute these changes to lateral confinement effects, which become important when the GaAs layer thickness aproaches the double step height $2\delta = 20.4$ Å (see Fig. 1). These effects will be further discussed in Sec. IV C.

The sharp lines are superimposed on a smooth structured background that also increases with decreasing layer thickness. The dependence on layer thickness suggests that the background is not related to the corrugation of the top surface of the sample. As will be seen in the following, this background also gives direct evidence for the corrugated nature of the superlattice interfaces.

IV. DISCUSSION

Two basic mechanisms contribute to the optical anisotropy in (311)-oriented superlattices. The first mechanism is interface related and associated with the presence of an oriented interface corrugation, as illustrated in Fig. 1. As will be discussed in Sec. IV A, this mechanism accounts for the structured background observed in Fig. 4. The second mechanism arises from the fact that the confinement effects on the electronic states of the superlattice layer depends on the in-plane **k** direction. We shall show in Sec. IV B that the effects of confinement on the valence band states can account for the sharp structures illustrated in Fig. 4. This conclusion is further supported by microscopic tight-binding calculations of the optical anisotropy to be presented in Sec. IV C.

A. Interface corrugation

The effect of the corrugation of Fig. 1 on the optical anisotropy can be understood using an effective medium approximation for the optical properties. When the electric field of the incoming light is perpendicular to the corrugation steps (i.e., **E** along [$\bar{2}$33]) the electromagnetic boundary conditions require the electric field to be continuous at the interfaces. If we neglect quantum confinements effects, the dielectric constant can be estimated from those of bulk GaAs (ϵ_{GaAs}) and AlAs (ϵ_{AlAs}) with an effective medium approximation. This approximation, which is valid in the limit of superlattice dimensions small compared to the light wavelength, yields a dielectric constant for polarization along the steps (i.e., the [$\bar{2}$33] direction) that is a weighted average between ϵ_{GaAs} and

ϵ_{AlAs}, given by:

$$\epsilon'_{[\bar{2}33]} = \frac{d_{GaAs}\epsilon_{GaAs} + d_{AlAs}\epsilon_{AlAs}}{d_{GaAs} + d_{AlAs}}, \qquad (2)$$

where a prime is used to distinguish the dielectric constant determined in the effective medium approximation from the measured one.

For an electric field perpendicular to the corrugation (i.e., along [$0\bar{1}1$]) the situation is more complicated, since the electric field is no longer continuous across the interface. An effective dielectric constant can still be obtained in the effective medium approximation by assuming the corrugation angle θ to be equal to 0° instead of the value of $\theta = 49.5°$ determined from transmission electron microscopy (see Fig. 1).[2,3] In this case, a simple calculation yield the following expression for the dielectric constant along [$0\bar{1}1$]:

$$\epsilon_{[0\bar{1}1]} \sim \frac{d_{GaAs}\epsilon_{GaAs} + d_{AlAs}\epsilon_{AlAs}}{d_{GaAs} + d_{AlAs}} \\ - \frac{\delta}{d_{GaAs} + d_{AlAs}} \frac{(\epsilon_{GaAs} - \epsilon_{AlAs})^2}{\epsilon_{GaAs} + \epsilon_{AlAs}}. \qquad (3)$$

The difference $\Delta\epsilon' = \epsilon'_{[0\bar{1}1]} - \epsilon'_{[\bar{2}33]}$ is then given by

$$\Delta\epsilon' \sim - \frac{\delta}{d_{GaAs} + d_{AlAs}} \frac{(\epsilon_{GaAs} - \epsilon_{AlAs})^2}{\epsilon_{GaAs} + \epsilon_{AlAs}}. \qquad (4)$$

As expected, $\Delta\epsilon'$ increases with the modulation amplitude and with the difference between the dielectric constant of the two media.

The dashed lines in Fig. 4 were calculated from Eq. (4), using the nominal superlattice layer thicknesses and the bulk dielectric constant for GaAs and AlAs.[25,22] The corrugation amplitude $\delta = 10.2$ Å was taken to be equal to the value determined by transmission electron microscopy (TEM).[3] As expected, the anisotropy from Eq. (4) increases as the ratio between the corrugation amplitude and the superlattice period decreases. Note that the dashed lines are scaled by a factor of 0.3 in Fig. 4 and, therefore, Eq. (4) overestimates by a factor of ~ 3 the experimental data.

The effective medium approximation reproduces most of the features observed in the structured background of the large period superlattice ($d = 127$ Å) of Fig. 4(d). In particular, the minimum at 3 eV and the broad maximum at 3.5 eV coincide with the experimental data. Although the same features are still present, the degree of agreement is less satisfactory for superlattices of smaller periods. This is probably due to the fact that the dielectric constant of the thin layers can no longer be described by the bulk values. The structured background thus evidences the corrugated nature of the superlattice interfaces.

The small amplitude (by a factor of ~ 3) of the measured background in comparison with the predictions of Eq. (4) is presently not well understood. The assumption of a squarelike profile for the corrugation steps used in the derivation of Eq. (4) overestimates the anisotropy, due to the higher electrostatic form factor in compari-

son with a smoother corrugation profile.[26] The overestimation, however, should not exceed a factor of 2. The ramaining differences between the experimental and calculated curves seems to be too large to be accounted for only by the simplifying assumptions leading to Eqs. (3) and (4). A possible explanation is the mixing of the GaAs-like and of the AlAs-like dielectric functions in the interface region, which is explicitly neglected in the effective medium treatment. Such a mixing will reduce the effective difference between the bulk dielectric constant in the interface region, and, therefore, the optical anisotropy. Note that a wave function penetration of only ~ 5 Å in the neighboring layer will effectively reduce the anisotropy, due to the 10 Å interface steps by a factor of 3 and bring Eq. (4) in better agreement with the experimental results. Another possibility is that the corrugation amplitude determined by TEM (Ref. 3) is not uniform, but varies over the sample area. The average value of the corrugation, in this case, should be a factor of ~ 3 smaller than the TEM value of $\delta = 10.2$ Å. This topic remains a subjet for further investigations.

B. Confinement effects

We turn now to the analysis of the sharp structures in $\Delta\varepsilon$ shown in Fig. 4. These structures appear in the energy range of the E_1 and $E_1 + \Delta_1$ transition in bulk GaAs (2.9 eV and 3.1 eV, respectively, at room temperature) and in AlAs (3.9 and 4.15 eV, respectively). The optical spectra of the bulk materials in this energy range is dominated by transitions between the lowest conduction band and the highest valence band states along the Γ line ($\langle 111 \rangle$ direction). The approach to be followed here, similar to that applied by Schmid et al.[4] for the analysis of the optical anisotropy in [011]-oriented superlattices, consists in determining the changes in the valence and conduction band GaAs (or AlAs) wave function due to the superlattice confinement.

We assume the reference frame X', Y', and Z' illustrated in Fig. 5(a) with the Z' axis oriented along the cation-anion ([111]) direction and neglect, for the moment, the effects of spin-orbit coupling. Along the Λ line [see solid line in the band structure of Fig. 5(b)], the lowest conduction band state has cylindrical symmetry around the Z' axis ($\Lambda_{6,c}$ symmetry). The upper valence band states, on the other hand, are twofold degenerate p-like states with symmetries X' and Y', respectively. The degeneracy of these states is lifted for wave vectors with a component in the direction perpendicular to the Λ line, as indicated by the dashed lines in Fig. 5(b). Along these directions, the Y'-like state is approximately dispersionless with a high effective mass, while the X'-like state has an effective mass $\sim 0.12 m_0$ ($m_0 \equiv$ free electron mass). The valence band degeneracy is also lifted in the presence of a confinement potential, e.g., in the X' direction. An infinite confinement potential $V(x)$,

$$V(x') = \begin{cases} 0, & |x'| \leq \frac{d}{2} \\ \infty, & |x'| > \frac{d}{2}, \end{cases} \tag{5}$$
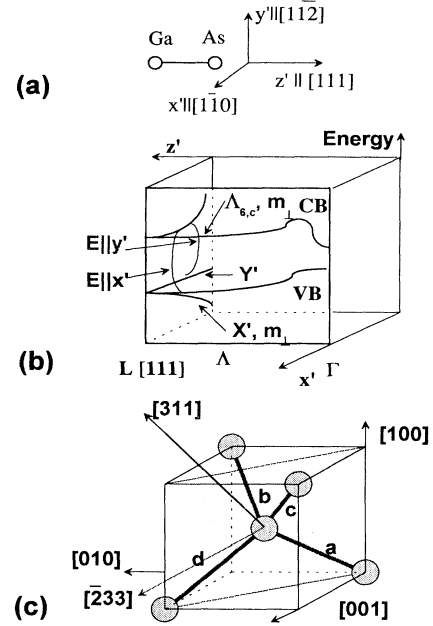
FIG. 5. (a) Reference frame with the z'-axis along the [111] direction, (b) Near-gap band structure of GaAs along the Λ direction. The X' and Y' valence band states are degenerate along the Λ line, while the degeneracy is lifted for directions perpendular to Λ, where the Y' state is practically dispersionless. The curved lines indicate the polarization dependence of the coupling between the valence states and the $\Lambda_{6,c}$-like conduction band. (c) Relative orientation of the bonds relative to the [311] axis.

splits the X'-like band valence band ($\Lambda_{6,c}$-like conduction band) in a series of states shifted by $-\frac{n^2\Delta E}{2}$ ($\frac{n^2\Delta E}{2}$), with respect to the bulk valence (conduction) band. Here,

$$\Delta E = \frac{\hbar^2}{m_{v\perp}} \left(\frac{\pi}{d_{\text{GaAs}}}\right)^2 \quad \left[\Delta E = \frac{\hbar^2}{m_{c\perp}} \left(\frac{\pi}{d_{\text{GaAs}}}\right)^2\right]$$

is the confinement shift for the valence (conduction) band with transverse (with respect to the [111] direction) mass $m_{v\perp}$ ($m_{c\perp}$). The expression for ΔE is valid in the limit $m_\perp \gg m_\parallel$. The Y'-like state, on the other hand, remains practically unaffected by the confinement, due to its large transverse mass. The optical anisotropy arises from the polarization dependence of the transitions elements between the confinement-split valence and conduction bands. For dipole-allowed transitions X'- (Y'-) polarized light only couples the X'-like (Y'-like) valence states to the $\Lambda_{6,c}$-like conduction band.

The discussion of the previous paragraphs can be readily extended to calculate the optical anisotropy of the GaAs layers in (311)-GaAs/AlAs superlattices. As illustrated in Fig. 5(c) the four {111} directions (denoted by a, b, c, and d, corresponding to $\mathbf{k}$ vectors L_a, L_b, L_c, and L_d, respectively) in this case are not equivalent with respect to the [311] confinement direction and do not lie along the layer plane. In order to determine the confinement shifts for each one of the {111} direc-

TABLE II. Energy shifts [in units of $\Delta E = \frac{\hbar^2}{m_\perp}\left(\frac{\pi}{d_{GaAs}}\right)^2$] and strengths of the E_1-like transitions in (311)-oriented superlattices for different orientations of the light electric field E. The shifts and transition strenghts were calculated using the bond polarizability model described in the text. The L-point vectors $L_a - L_d$ correspond to the bond directions $a - d$ indicated in Fig. 5(b).

Direction/k-vector	$L_a - [111]\frac{\pi}{a_0}$	$L_b - [\bar{1}\bar{1}1]\frac{\pi}{a_0}$	$L_c - [\bar{1}1\bar{1}]\frac{\pi}{a_0}$	$L_d - [1\bar{1}\bar{1}]\frac{\pi}{a_0}$
Energy shift	$\frac{3}{33}$	$\frac{9}{33}$	$\frac{9}{33}$	$\frac{12}{33}$
$E_\parallel[0\bar{1}1]$	$\frac{1}{2}$	$\frac{1}{6}$	$\frac{1}{6}$	$\frac{1}{2}$
$E_\parallel[\bar{2}33]$	$\frac{25}{66}$	$\frac{31}{66}$	$\frac{31}{66}$	$\frac{1}{66}$
$[0\bar{1}1] - [\bar{2}33]$	$\frac{4}{33}$	$-\frac{10}{33}$	$-\frac{10}{33}$	$\frac{16}{33}$

tion one must first calculate the projection of the wavefunctions along the confinement direction. The resulting confinement shifts and relative matrix elements for optical transitions near the L point are summarized in Table II. The transition elements, determined for incident polarization along the main in-plane axes $[0\bar{1}1]$ and $[\bar{2}33]$, are expressed in units of the bulk transition element $P^2 = |\langle X'|p_{x'}|\Lambda_{6,c}\rangle|^2$ between the valence and conduction states at the L point. The calculations assumed infinite confinement barrier and a ratio $m_{c\perp}/m_{v\perp} = 2$ between the conduction and valence band at the L point. The mixing of the X' and Y' valence band state due to spin-orbit coupling was also taken into account. As a consequence of the mixing the same energy shifts and matrix elements are expected for the E_1 and $E_1 + \Delta_1$ bulk states.

Table II indicates that the confinement yields the same energy shifts (and also same transition elements) for the $\{111\}$ states oriented along directions b and c [see Fig. 5(c)]. This results from the same orientation of the bond b and c, with respect to the confinement [311] axis. The smallest (largest) energy shifts are found for direction a (d). This direction is almost parallel (perpendicular) to the [311] direction so that the confinement effects is minimal (maximal). The optical anisotropy [see lowest curve in Fig. 5(d)] results mainly from the contribution from $\{111\}$ states along b, c, and d.

The simple model presented above provides a physical insight into the origin of the anisotropy. It is also in qualitative agreement with the experimental data of Fig. 4 near the bulk GaAs E_1 gap (indicated by the vertical line at 2.9 eV in Fig. 4), with $\Delta\varepsilon_2 = \varepsilon_{2,[0\bar{1}1]} - \varepsilon_{2,[\bar{2}33]}$ going through a minimum (due to the anisotropy of the L_b and L_c states) and then through a maximum (due to the L_d states) with increasing energy above the E_1 transition energy. The validity of the model will be further discussed in Sec. IV D.

C. Tight-binding calculations

In order to obtain a closer insight on the optical anisotropy, we performed microscopic calculations of the superlattice dielectric constant using the empirical tight-binding method (ETB). The calculations used a basis consisting of sp^3s^* orbitals,[27] with and without spinorbit coupling.[28,29] The matrix elements for the tight-binding

Hamiltonian were extracted from Refs. 27 and 29. A valence band offset 0.5 eV was subtracted from the on-site elements of the AlAs tight-binding Hamiltonian in order to simulate the valence band discontinuity between GaAs and AlAs (top of valence band higher in GaAs). The Hamiltonian matrix elements for the interface As atom between two consecutive layers were taken to be the average of the corresponding values in GaAs and AlAs. The calculations were performed for structures with flat interfaces.

The imaginary part of the dielectric function projected along a given polarization direction was calculated by performing a random sampling over the superlattice Brillouin zone. Typically, 1000 random points were used for a superlattice with 64 atoms per unit cell, corresponding to a period of 54.4 Å. More points were used for samples with smaller unit cell or in the cases where the spin-orbit coupling was neglected. The optical transition elements were obtained directly from the tight-binding Hamiltonian, using the procedure described in Refs. 30 and 31. The optical anisotropy Im$(\Delta\varepsilon)$ was then obtained from the difference of the dielectric tensor components along the $[0\bar{1}1]$ and $[\bar{2}33]$ in-plane directions.

The tight-binding results for the optical anisotropy are summarized in Fig. 6 for superlattices with layer thicknesses of 13.6 Å/13.6 Å [Fig. 6(a)] and 27.2 Å/27.2 Å [Fig. 6(b)] (the energy scale is shown in the upper part of the plot). The thick and thin lines displays the calculated $\Delta\varepsilon_2 = \text{Im}[\varepsilon_{[0\bar{1}1]} - \varepsilon_{[\bar{2}33]}]$ including and neglecting the spin-orbit interaction, respectively. The same tight-binding parameters were used in both calculations, except for those describing the spin-orbit interaction. As a result, the calculated E_1 transition energy is slightly redshifted ($\sim$ 0.1 eV) when the spin-orbit interaction is taken into account. The dashed and dot-dashed vertical lines in Fig. 6(a) and (b) indicate the calculated energy of the E_1 and $E_1 + \Delta_1$ transitions in bulk GaAs. Apart from small energy shifts, the overall spectral shape does not change appreciably with the superlattice period. A pronounced anisotropy is observed near the GaAs E_1 and $E_1 + \Delta_1$ transitions. Note that the minimum near $E_1 + \Delta_1$ is only seen when the spin-orbit interaction is included in the calculation, in agreement with these assignment. The anisotropy is higher by a factor of $\sim$ 2 in the former caser, further indicating the importance of the spin-orbit effects for the optical anisotropy.

0.7 1.7 2.7 3.7 4.7

1 2 3 4 5
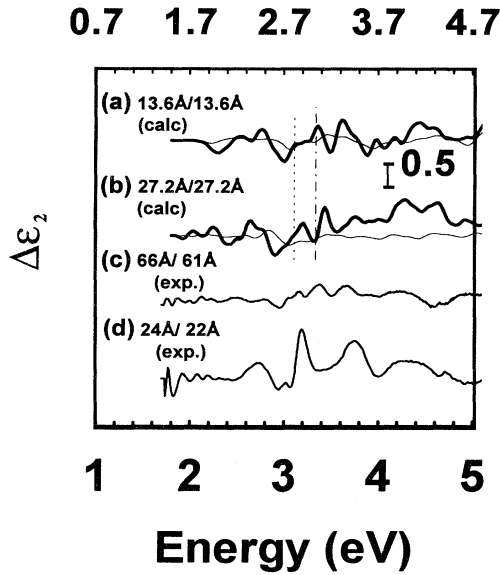
Energy (eV)

FIG. 6. $\mathrm{Im}[\Delta\varepsilon] = \mathrm{Im}[\varepsilon_{[0\bar{1}1]} - \varepsilon_{[\bar{2}33]}]$ calculated using the tight-binding method including (thick lines) and neglecting (thin lines) the spin-orbit interaction for (311)-oriented GaAs/AlAs superlattices with layer thicknesses of (a) 13.6 Å/13.6 Å (upper energy scale) and (b) 27.2 Å/27.2 Å (upper energy scale). Measured anisotropy spectrum for (c) a 66 Å/61 Å GaAs/AlAs samples (lower energy scale) and for a (d) 22 Å/24 Å GaAs/AlAs superlattice (lower energy scale). The dotted and dot-dashed vertical lines indicate the energy of the E_1 and $E_1 + \Delta_1$ transitions in bulk GaAs, such as *calculated* by the tight-binding method. The calculated curves, which neglect the interface corrugation, are in better agreement with the anisotropy measured in samples with large GaAs layer thickness.

Figure 6(c) shows for comparison the measured anisotropy spectrum for a 66 Å/61 Å GaAs/AlAs samples (unfortunately, the large computation time restricts the calculation to structures with period smaller than ∼ 50 Å) and for a 22 Å/24 Å GaAs/AlAs samples. The calculated and measured spectra in Fig. 6 were shifted relative to each other in order to account for the differences between the calculated and measured critical point energies (see upper and lower energy scales in the figure). The calculated spectra reproduce fairly well the experimental results for the sample with large layer thicknesses. Since the calculations do not take into account the interface corrugation, we conclude that the sharp lines observed in large period samples [i.e., periods > 80 Å, see Fig. 4(c) and (d)] are not related to the interface corrugation.

The anisotropy spectra measured on short period samples [Fig. 6(d)], on the other, cannot be reproduced by the tight-binding calculations. This discrepancy is attributed to the effects of lateral confinement in samples with layers thicknesses comparable to the corrugation amplitude.

Finally, the tight-binding results can be used to check the valid of the simple model for the anisotropy discussed in Sec. IV C for the confinement effect on the {111} bulk

states. For this purpose, we calculate, using the tight-binding method, the transition energies and the transition matrix elements for the bulk states L_a to L_d corresponding to the bond directions a–d of Fig. 5(c). The anisotropy of the squared matrix elements (i.e., their difference for polarization along the $[0\bar{1}1]$ and $[\bar{2}33]$ in-plane directions) is plotted as a function of the transition energy in Figs. 7(a), 7(b), and 7(c) for the states L_a, L_b and L_c, and L_d. The calculations were performed for a 27.2 Å/27.2 Å GaAs/AlAs superlattice, including the spin-orbit interaction. As a consequence of the symmetry arguments described before, states L_b and L_c have the same matrice elements and are represented by a single curve in Fig. 7(b). Note that the superlattice periodicity can fold non-{111} states into {111}-superlattice states: the corresponding transition matrix elements are also displayed in in Figs. 7(a–c). As an example, the bulk state L_d is folded into the Γ point for superlattices with period containing a number of monolayers multiple of 4 (as happened to be the case of Fig. 7). The transition elements for energies below 2.5 eV in Fig. 7(c) are due to transition associated with Γ-like superlattice states.

The vertical dashed lines in the plot indicate the calculated position of the E_1, and $E_1 + \Delta_1$ transitions of bulk GaAs. In agreement with the results of Sec. IV B (see Table II), the energy shift from the bulk E_1 transition due to confinement increases in the order $L_a \to L_b(= L_c) \to L_d$ [see solid arrows in Fig. 7(a–c)]. The onset of the superlattice $E_1 + \Delta_1$-like transitions (dashed arrows) is not as well defined as in the previous case, but seems to
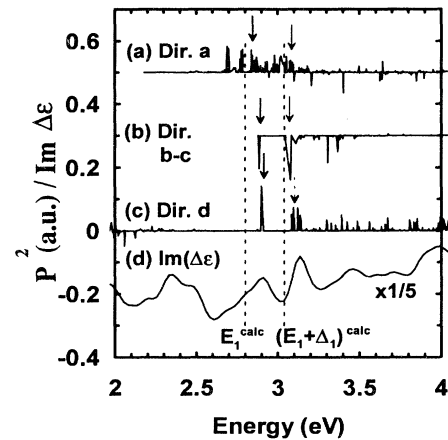
FIG. 7. Difference between the squared matrix elements for optical transition between the valence and conduction band for polarization along $[0\bar{1}1]$ and $[\bar{2}33]$. The calculations were performed using the tight-binding method for a 27.2 Å/27.2 Å (311)-oriented GaAs/AlAs superlattice including spin-orbit coupling, for **k** vectors corresponding to different bulk {111} directions: (a) $L_a = [111]\frac{\pi}{a_0}$, (b) $L_b = [\bar{1}\bar{1}1]\frac{\pi}{a_0}$ (equivalent to $L_c = [111]\frac{\pi}{a_0}$), and (c) $L_d = [\bar{1}11]\frac{\pi}{a_0}$. (d) Calculated dielectric anisotropy $\mathrm{Im}[\Delta\varepsilon] = \mathrm{Im}[\varepsilon_{[0\bar{1}1]} - \varepsilon_{[\bar{2}33]}]$ for the same sample. The curves are shifted vertically for clarity. The vertical dashed lines indicate the calculated position of the E_1 and $E_1 + \Delta_1$ transitions of bulk GaAs. The arrows in (a)–(c) shows the calculated onset of the E_1-like and $(E_1 + \Delta_1)$-like superlattice transitions.

follow the same behavior. The sign of the polarization anisotropy at the onset of the transitions, negative for L_b and L_c and positive for the other transitions, is also in agreement with Table II.

Figure 7(d) reproduces for comparison the *calculated* anisotropy of the imaginary part of the dielectric function for the same sample. We recall that since the dielectric function is calculated by sampling the whole Brillouin zone it depends not only on the matrix elements but also on the joint density of states at the different **k** points. By comparing the structures in Fig. 7(d) with the transition elements, one can verify that the spectral features in the E_1 and $E_1+\Delta_1$ range (2.8–3.8 eV) can be well reproduced by taken into account only the Λ-like transitions.

V. CONCLUSIONS

We have investigated the optical anisotropy of (311)-oriented GaAs/AlAs superlattices in the energy range from 2–5.5 eV. The spectral dependence of $\Delta\varepsilon = \varepsilon_{[0\bar{1}1]} - \varepsilon_{[\bar{2}33]}$ is characterized by sharp peaks (FWHM~ 0.15 eV) superimposed on a structured background. In samples with period large than 80 Å , the sharp lines are mainly due to the vertical confinement of the GaAs layers. This conclusion is supported by tight-binding calculations of the optical anisotropy performed neglecting interface corrugation. The changes in the spectral shape for smaller periods are attributed to the increasing role of lateral confinement. These conclusions are in agreement with results for the optical anisotropy near the fundamental gap.[8] The structured background, on the other hand, is attributed to the interface corrugation. The spectral shape of the background is reproduced by an effective medium approximation for the optical anisotropy, presented in Sec. IV A, which takes into account the amplitude of the surface corrugation and the dielectric constant of the layers. We found, however, that the measured anisotropy is a factor of ~ 3 smaller than that expected from the amplitude of the corrugation.

* On leave from Departamento de Física Aplicada, Universidad de Valencia, Burjasot, E-46100 Valencia, Spain.

† Present address: Paul-Drude-Institut für Festkörperelektronik, Hausvogteiplatz 5-7, D-10117 Berlin, Germany.

[1] L.N. Pfeiffer, K.W. West, H.L. Stormer, J. Eisenstein, K.W. Baldwin, D. Gershoni, and J. Spector, Appl. Phys. Lett. **56**, 1697 (1990).

[2] R. Nötzel, N. Ledentsov, L. Däweritz, M. Hohenstein, and K. Ploog, Phys. Rev. Lett. B **27**, 3507 (1991).

[3] R. Nötzel, N.N. Ledentsov, L. Däweritz, K. Ploog, and M. Hohenstein, Phys. Rev. B **45**, 3507 (1992).

[4] U. Schmid, N.E. Christensen, M. Cardona, F. Lukes, and K. Ploog, Phys. Rev. B **45**, 3546 (1992).

[5] S. Nojima, Jpn. J. Appl. Phys. **31**, L765 (1992).

[6] S. Nojima, Phys. Rev. B **47**, 13 535 (1993).

[7] D. Gershoni, I. Brener, G.A. Baraff, S.N.G. Chu, L.N. Pfeiffer, and K. West, Phys. Rev. B **44**, 1930 (1991).

[8] M.V. Belousov, V.L. Berkovits, A.O. Gusev, E.L. Ivchenko, P.S. Kop'ev, N.N. Ledensov, and A.I. Nesvizhskii, Phys. Solid State **36**, 596 (1994).

[9] G. Armelles, P. Castrillo, P.S. Domíngues, L. González, A. Ruiz, D.A. Contreras, V.R. Velasco, and F. García-Moliner, J. Phys. (France) IV **5**, C283 (1994).

[10] G. Armelles, P. Castrillo, P.S. Domíngues, L. González, A. Ruiz, D.A. Contreras, V.R. Velasco, and F. García-Moliner, Phys. Rev. B **49**, 14 020 (1994).

[11] Y. Hsu, W.I. Wand, and T.S. Kuan, Phys. Rev. B **50**, 4973 (1994).

[12] A. Orth, J.P. Reithmayer, A. Forchel, R. Nötzel, and K. Ploog, Appl. Phys. Lett. **64**, 3443 (1994).

[13] S.-S. Li and J.-B. Xia, Phys. Rev. B **50**, 8682 (1994).

[14] G. Armelles, P. Castrillo, P.D. Wang, C.M Sotomayor Tor-res, N.N. Ledensov, and N.A. Bert, Solid State Commun. **94**, 613 (1995).

[15] D.A. Contreras-Solorio, V.R. Velasco, and F. García-Moliner, Phys. Rev. B **47**, 4651 (1993).

[16] Z.V. Popović, E. Richter, J. Spitzer, M. Cardona, A.J. Shields, R. Nötzel, and K. Ploog, Phys. Rev. B **49**, 7577 (1994).

[17] A.J. Shields, Z.V. Popović, M. Cardona, J. Spitzer, R. Nötzel, and K. Ploog, Phys. Rev. B **49**, 7584 (1994).

[18] Z. Ikonić, G.P. Srivastava, and J.C. Inkson, Phys. Rev. B **49**, 10 749 (1994).

[19] E. Ribeiro and F. Cerdeira (private communication).

[20] D.E. Aspnes, J.P. Harbison, A.A. Studna, and L.T. Flores, J. Vac. Sci. Technol. A **6**, 1327 (1988).

[21] D.E. Aspnes, J. Opt. Soc. Am. **70**, 1275 (1980).

[22] M. Garriga, Ph.D. thesis, University of Stuttgart, 1990.

[23] P.V. Santos, P.E. Etchegoin, M. Cardona, B. Brar, and H. Kroemer, Phys. Rev. B **50**, 8746 (1994).

[24] D.E. Aspnes, J. Vac. Sci. Technol. B **3**, 1498 (1985).

[25] D.E. Aspnes and A.A. Studna, Phys. Rev. B **27**, 985 (1983).

[26] L.D. Landau and E.M. Liftshitz, *Electrodynamics of Continous Media* (Pergamon Press, Oxford, 1963), p. 42.

[27] P. Vogl, H. Hjalmarson, and J. Dow, J. Phys. Chem. Solids **44**, 365 (1983).

[28] K.C. Hass, H. Ehrenreich, and B. Velický, Phys. Rev. B **27**, 1088 (1983).

[29] D.J. Chadi, Phys. Rev. B **16**, 790 (1977).

[30] G. Dresselhaus and M.S. Dresselhaus, Phys. Rev. **160**, 649 (1967).

[31] L.C. Lew Yan Voon and L.R. Ram-Mohan, Phys. Rev. B **47**, 15 500 (1993).